RSC Advances

PAPER

View Article Online
View Journal | View Issue

Cite this: *RSC Adv.*, 2020, **10**, 23582

Comparative investigations of *in vitro* and *in vivo* bioactivity of titanium *vs.* Ti–24Nb–4Zr–8Sn alloy before and after sandblasting and acid etching

Xin Liu,[a] Yumei Niu, †*[b] Weili Xie,†*[a] Daqing Wei[c] and Qing Du[c]

Received 10th January 2020
Accepted 22nd May 2020

DOI: 10.1039/d0ra00280a

rsc.li/rsc-advances

To avoid the failure of clinical surgery due to "stress shielding" and the loosening of an implant, a new type of alloy, Ti–24Nb–4Zr–8Sn (TNZS), with a low Young's modulus acted as a new implant material in this work. Meanwhile, the surface characteristics, MC3T3-E1 cell behavior and *in vivo* osseointegration of the titanium and TNZS before and after sandblasting and acid etching were studied comparatively. TNZS and Ti had the same microstructure based on the transmission electron microscopy results. Meanwhile, the TNZS alloy had a lower Young's modulus and surface nanohardness compared with pure titanium. However, the corrosion resistance of Ti was better than that of the TNZS sample in simulated body fluid solution. In addition, the TNZS alloy after sandblasting and acid etching (SLATNZS) had excellent cell adhesion, proliferation, differentiation, ALP activity and *in vivo* osseointegration ability such as there being almost no soft tissue as compared with other implants. Based on the current results, the new type of Ti–24Nb–4Zr–8Sn alloy showed good potential and promising application prospects in its biochemical aspects.

1. Introduction

Titanium and its alloys show potential in hard tissue repair and replacement due to their good biocompatibility and good corrosion resistance.[1,2] Meanwhile, titanium and its alloys possess excellent mechanical properties, while their high Young's modulus could lead to stress shielding after implantation, which could result in the absorption of native bone tissue around the titanium implants.[3–5] Thus, researchers have developed a new β-type, Ti–24Nb–4Zr–8Sn (TNZS) for biological applications. It has a lower Young's modulus (about 33 GPa, close to that of human bone) than that of the typical α + β type Ti–6Al–4V alloy (120 GPa) or pure titanium (103.4 GPa), which could avoid "stress shielding" between the native bone and the implant.[6–10] Thus, the TNZS alloy has attracted more researchers' attention.

As is well known, the sandblasting and acid-etching method (SLA) has been widely used in the surface modification of dental titanium implants, and SLA treated dental titanium implants have been successfully applied clinically. However, these still take place in clinical surgery. Moreover, previous studies had reported that surface characteristics such as surface wettability, roughness, surface topology and surface chemistry played an important role in new bone construction during healing. In detail, the micro-scale and sub-micro-scale topological structures played an important role in bone remodeling at an early stage of healing,[11] which could promote the mechanical interlocking between the implant and native bone, thus retaining the stability of the implant. Besides, the sub-micro and micro-scale structures had similar sizes of cell dimensions and absorption pits, leading to the adhesion and proliferation of osteoblasts *in vitro* and enhancement of bone-to-implant contact *in vivo*.[12] In past decades, some studies reported that a nano-scale surface structure can enhance the osteoblast response behavior and gene expression.[12–16] Meanwhile, the suitable wettability and roughness on the implant surface had a critical role in the interaction between the biomaterial and the bioenvironment, especially water and protein, and further influenced cell behavior.[17–19] Thus, a hierarchical micro–nano-scale topological structure with suitable surface roughness and wettability could effectively achieve excellent cell biomaterial interaction at an early stage of healing. In this work, the common surface modification method (the SLA method) was applied to change the surface structure of the titanium and TNZS plates. The surface characters of the titanium and TNZS plates before and after SLA treatment, such as wettability, roughness, Young's modulus and hardness, were studied comparatively. Meanwhile, the MC3T3-E1 cell response behavior and *in vivo* osseointegration of the titanium and TNZS before and after SLA treatment were also studied.

[a]*Department of Prosthodontics, The First Affiliated Hospital of Harbin Medical University, Harbin, Heilongjiang Province, China. E-mail: xwl811@126.com*

[b]*Department of Endodontics, The First Affiliated Hospital of Harbin Medical University, Harbin, Heilongjiang Province, China. E-mail: niuyumei@hrbmu.edu.cn*

[c]*Harbin Institute of Technology School of Materials Science and Engineering, Harbin, Heilongjiang Province, China*

† These authors contributed equally to this work.

2. Materials and methods

2.1 Preparation and characterization of materials

2.1.1 Material preparation. The *in vitro* test employed Ti and TNZS sheets ($10 \times 10 \times 1$ mm^3), and the *in vivo* experiment employed Ti and TNZS cylindrical rods (φ 2 $\times$ 6 mm^3). Our previous study reported in detail the sandblasting and acid-etching parameters and processes.[20] The Ti and TNZS sheets and rods treated by sandblasting and acid etching were named SLATi and SLATNZS.

2.1.2 Structure characterization. In this work, we studied the surface morphologies, chemical compositions and microstructures of the Ti and TNZS samples by scanning electron microscopy (SEM, Helios NanoLab 600i, FEI Co., USA) and transmission electron microscopy (TEM, Talos F200x, FEI Co. USA) with an acceleration voltage of 200 kV. The surface wettability and roughness of the Ti and TNZS samples before and after sandblasting and acid etching were studied comparatively, and the measuring method and process were described in detail in our previous reports.[20,21]

The potentiodynamic polarization tests of pure Ti and Ti2448 plates before and after MAO treatment were performed on a Gamry 600 (Reference 600, Gamry, USA) electrochemistry workstation. Each of the samples (exposed area of 0.3 cm^2) was immersed into a conventional three-electrode cell containing the simulated body fluid (SBF) solution under open conditions to act as the working electrode, a platinum plate as the auxiliary electrode and a saturated calomel electrode (SCE) as the reference. After a 5 min delay under open conditions, the samples reached a stable state. The potentiodynamic polarization curves were measured from +1 V to −1 V according to the open circuit potentials (referenced to the SCE) with a scanning rate of 1 mV S^{-1}.

2.1.3 Nanoindentation test. The surface nanohardness and Young's modulus of the Ti and TNZS plates were measured using the nanoindentation test (G200, Agilent, USA) with a well-calibrated Berkovich diameter indenter. The process and parameters of the nanoindentation test were shown in detail in our previous study.[22,23]

2.2 *In vitro* studies

2.2.1 Cell culture. MC3T3-E1 cells were purchased from the Cell Bank of the Chinese Academy of Sciences. They were cultured at a density of 5×10^5 ml^{-1} on the Ti, TNZS, SLATi and SLATNZS samples for different amounts of time. Our previous investigations demonstrated the cell culture experiment and study method in detail.[23]

2.2.2 Cell adhesion and proliferation. For cell adhesion, after culturing for 1, 2 and 4 h, the OD values of the cultured solution containing the cells were used to evaluate the cell adhesion ability on the samples. In the case of cell proliferation, after culturing for 1, 3, 5 and 7 days, the cell proliferation ability on the samples was evaluated by detecting the OD value of the cultured solution containing the cells at a wavelength of 450 nm.

2.2.3 Alkaline phosphatase (ALP) activity and mineralization assay. For ALP activity, after culturing for 7 and 14 days, the ALP activity on the samples was evaluated by detecting the OD value of the cultured solution containing the cells at a wavelength of 520 nm. After culturing for 14 days, the absorbance of a solution containing Alizarin red was measured at 620 nm.

2.3 *In vivo* animal experiment

The animal experiments used in this study were approved by the Ethics Committee of the First Affiliated Hospital of Harbin Medical University, and were carried out under the control of the University's Guidelines for Animal Experimentation. The *in vivo* implantation surgery process and study methods were reported in detail in our previous investigations.[23] In this study, fifteen New Zealand rabbits with weight of 2.5–3 kg each were studied. Then, the Ti, TNZS, SLATi and SLATNZS implants were placed into four machined holes with size of ϕ 2 $\times$ 6 mm^3 on the tibias of the rabbits. The interfacial bonding status between the implant and bone was evaluated using the X-ray radiographic technique (DHF-155HII, Hitachi, Japan) and micro-computed tomography (Micro-CT, Siemens Co., America), Materialise's interactive medical image control system 20 (MINICS 20, Materialise Co., Belgium), and VG stained cross-sectional histological analysis.

2.4 Statistical analysis

SAS 6.0 software was used to perform the statistical analysis, and the data had statistical significance when $p < 0.05$. All the *in vitro* and *in vivo* experiments and surface characterizations were quantified with at least three independent replicates.

3. Results

3.1 Characterization of materials

3.1.1 SEM observation and EDS analysis. Fig. 1A shows the SEM images and EDS analysis of the Ti and TNZS samples before and after sandblasting and acid etching. For the Ti sample (in Fig. 1A(a) and (b)), after sandblasting and acid etching, a rough and porous surface was found on the SLATi sample surface. The EDS result suggested that the elemental composition of the SLATi sample included Ti element and a small amount of O element. In Fig. 1A(c) and (d), the SLATNZS sample became rougher compared with the flat TNZS sample. Moreover, the EDS spectrum revealed that the main elements of the SLATNZS sample were Ti, Nb, Zr and Sn, which was in agreement with those elements of TNZS before the sandblasting and acid etching.

3.1.2 TEM analysis. Fig. 1B shows the typical TEM and diffraction images of the Ti and TNZS samples and EDS elemental mapping distributions of Ti, Nb, Zr and Sn elements in the TNZS sample. In Fig. 1B(a) and (b), the diffraction result and TEM images confirmed that the microstructure of the Ti plate was composed of the equiaxed α-Ti phase, and the microstructure of the TNZS sample consisted of the equiaxed β-Ti phase (Fig. 1B(c) and (d)). The element mapping distribution of Ti, Nb, Zr and Sn elements is shown in Fig. 1B(e)–(h). It can

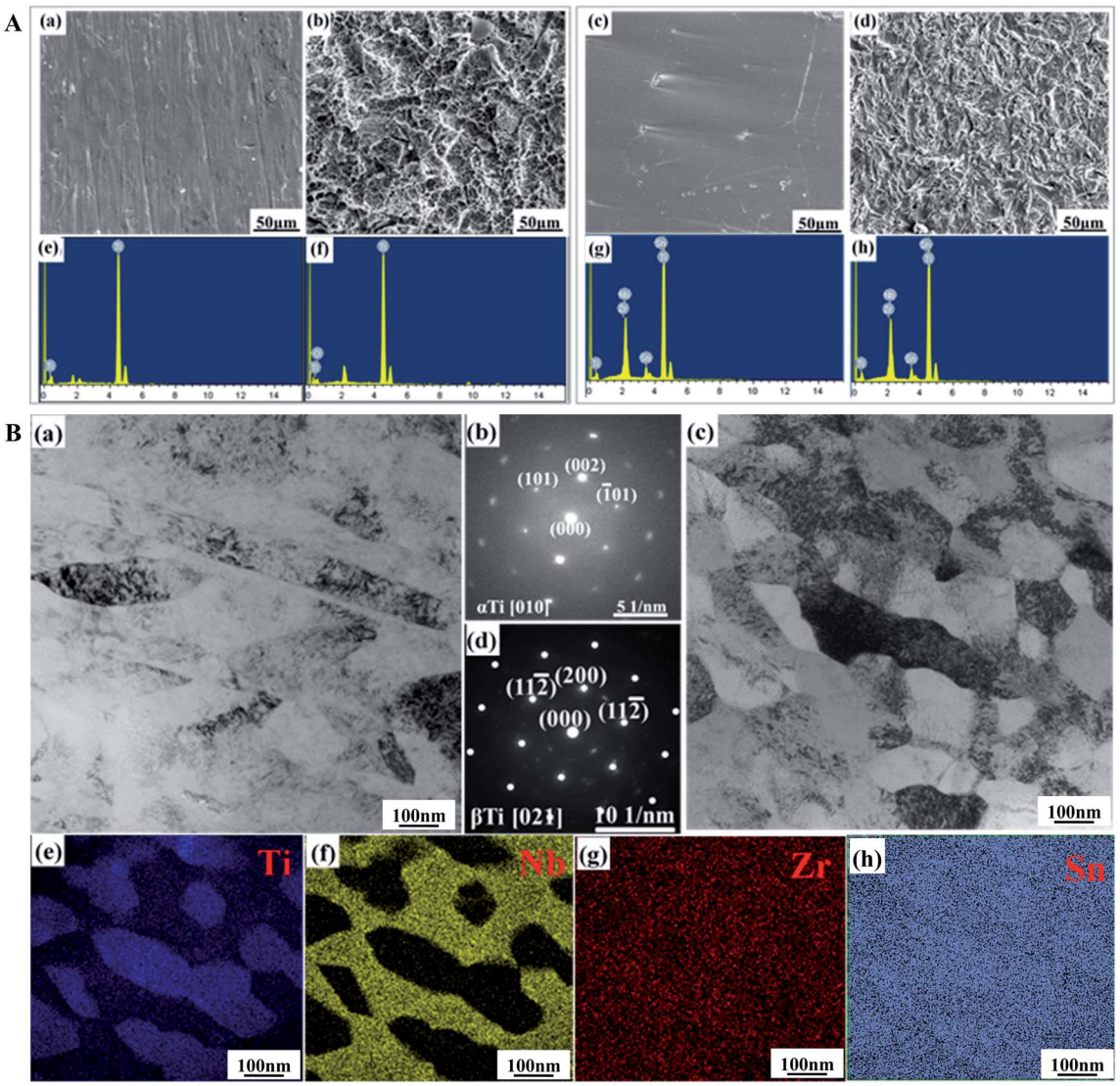

Fig. 1 Characterization of materials. (A) SEM observation and EDS analysis: (a) Ti sample, (b) SALTi sample, (c) TNZS sample, (d) SLATNZS sample, (e) the EDS spectrum of Ti, (f) the EDS spectrum of Ti, (g) the EDS spectrum of Ti and (h) the EDS spectrum of Ti. (B) TEM analysis: (a) a typical TEM image of a Ti sample, (b) the diffraction image of a Ti sample, (c) a typical TEM image of a TNZS sample, (d) the diffraction image of a TNZS image, (e)–(h) the EDS elemental mapping distributions of Ti, Nb, Zr and Sn elements in a TNZS sample.

clearly be seen that the distributions of Zr element in the TNZS sample are relatively homogeneous, while there is a clear boundary between the distributions of Ti, Nb and Sn elements, and Ti-rich, Nb-rich and Sn-rich regions exist in the microstructure of the TNZS sample.

3.1.3 Wettabilty and roughness. Fig. 2A shows the roughness and contact angle of the Ti and TNZS samples before and after sandblasting and acid etching. For the flat Ti and TNZS samples, after sandblasting and acid etching, the surface of the SLATi and SLATNZS samples became rougher. However, the contact angle for the Ti and TNZS samples before and after sandblasting and acid etching showed no significant increase, suggesting that the post treatment had no significant effect on the wettability.

3.1.4 Mechanical property. Fig. 2B shows the Young's modulus and nanohardness of the Ti and TNZS samples. It was clearly found that the Young's modulus of the Ti sample was about 130 GPa, which was higher that of the TNZS sample (about 23 GPa). Meanwhile, the hardness on the TNZS sample surface had declined slightly compared with that on the Ti sample surface.

Fig. 2C illustrates the open circuit voltage, impedance modulus, Nyquist plot and potentiodynamic curves of the Ti and TNZS samples in SBF solution. In Fig. 2C(a), it was clearly found that the open circuit voltage of the TNZS sample was greater than that of the Ti sample. In Fig. 2C(b), it can clearly be seen that the Z modulus of TNZS sample is lower than that of the Ti sample in the range of 0.01–100 000 Hz. In Fig. 2C(c), the Nyquist plots showed that the radius of curvature for pure Ti2448 (150 kΩ cm^2) was larger than that for pure Ti (250 kΩ cm^2), revealing that the corrosion resistance for pure Ti was better than that for pure Ti2448. The potentiodynamic

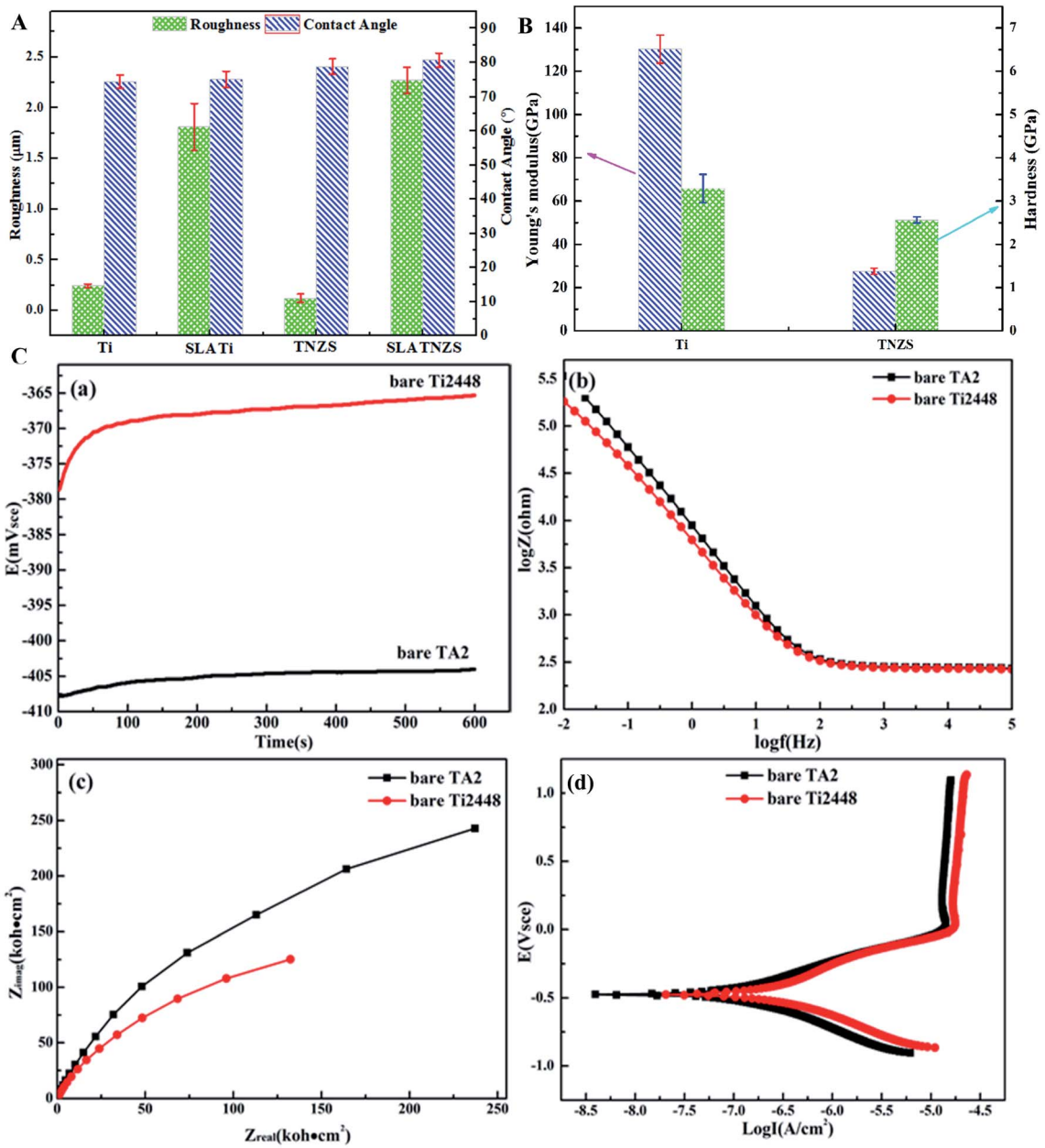

Fig. 2 Property of materials. (A) The roughness and contact angle of the Ti and TNZS samples before and after sandblasting and acid etching. (B) The Young's modulus and contact hardness of the Ti and TNZS samples. (C) The open circuit voltage, impedance modulus, Nyquist plot and potentiodynamic curves of the Ti and TNZS samples in SBF solution: (a) open circuit voltage, (b) impedance modulus, (c) Nyquist plot, (d) potentiodynamic curves.

polarization curves for pure Ti and Ti2448 are shown in Fig. 2C(d). It was clearly found that the pure TNZS samples had the same corrosion potentials as the Ti sample (−0.466 V and −0.466 V), while its corrosion current density was higher than that of the Ti sample (1.90×10^{-8} A cm^{-2} and 3.64×10^{-9} A cm^{-2}). As a result, the Nb, Zr and Sn elements in the TNZS sample were not effective in improving the corrosion resistance.

3.2 Results of *in vitro* studies

3.2.1 MC3T3-E1 cell adhesion. Fig. 3A shows the cell adhesion abilities of MC3T3-E1 cells on the Ti and TNZS sample surfaces after culturing for 1, 2 and 4 h. After culturing for 1 h, the cell adhesion on the Ti and TNZS samples was slightly higher than that on the SLATi and SLATNZS samples. With an increase in the culture time, the cell adhesion ratios showed no obvious increase on any sample surfaces. When the culture time was further increased to 4 h, the cell adhesion ratios on all sample surfaces showed an obvious increase, and those on the Ti and TNZS specimen were greater than those on the SLATi and SLATNZS sample surfaces. Based on this result, the relationship between a rough surface and cell adhesion ability was not very clear.

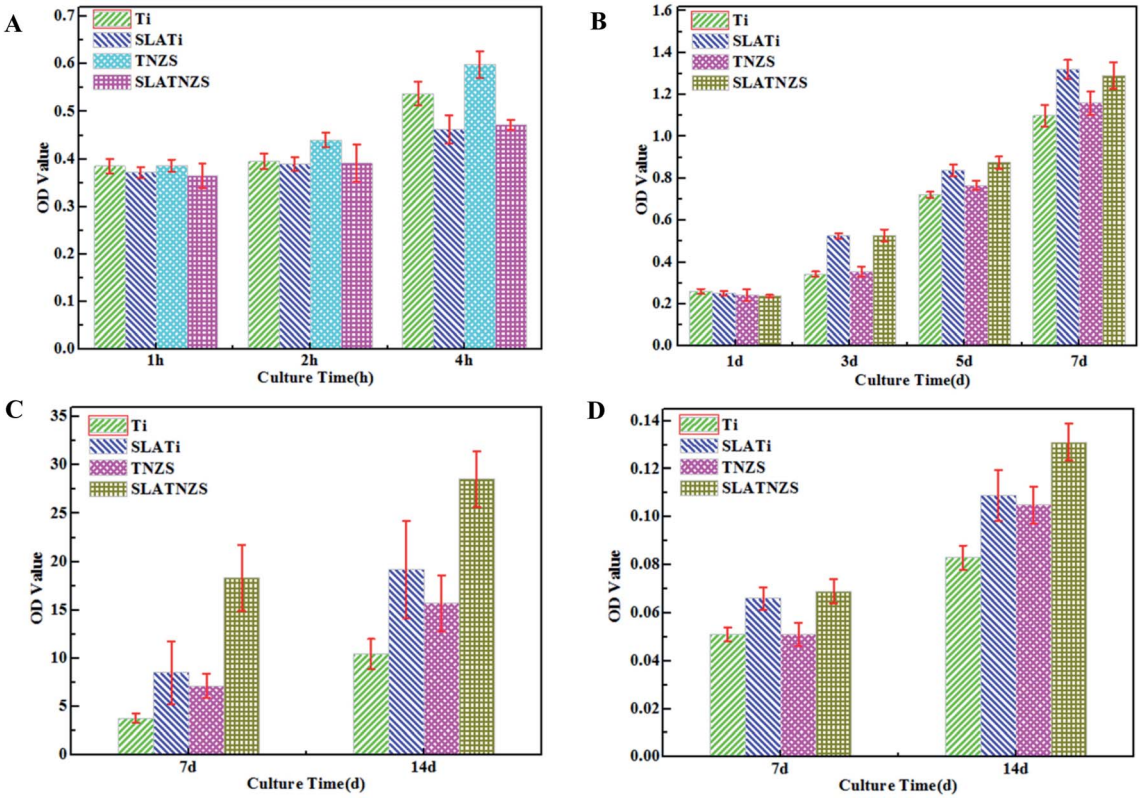

Fig. 3 Data from *in vitro* cell experiments. (A) MC3T3-E1 cell adhesion. (B) MC3T3-E1 cell proliferation. (C) ALP activity. (D) Alizarin red staining.

3.2.2 Cell proliferation. Fig. 3B represents the cell proliferation ability of MC3T3-E1 cells on the Ti and TNZS samples before and after sandblasting and acid etching after culturing for 1, 3, 5 and 7 d. After culturing for 1 d, the cell proliferation ability showed no significant difference on any sample surface. However, when the culture time was increased to 3, 5 and 7 d, the SLATi and SLATNZS samples had better cell proliferation ability than the flat Ti and TNZS sample surfaces, indicating that a rough surface was beneficial to cell proliferation.

3.2.3 ALP activity. Fig. 3C shows the ALP activity on the Ti and TNZS samples before and after sandblasting and acid etching after culturing for 7 and 14 d. It was clear that the ALP activity on the surface of the TNZS sample was better than that on the surface of the Ti sample, indicating that the TNZS sample with a low Young's modulus and hardness was beneficial to cell response. Moreover, the ALP activities on the SLA treated Ti and TNZS samples were better than those on the flat Ti and TNZS samples. However, the improvement in the ALP activity for the SLATNZS sample was much higher than that for the SLATi sample.

3.2.4 Alizarin red staining. Fig. 3D illustrates the OD values of MC3T3-E1 cells cultured on the Ti, TNZS, SLATi and SLATNZS samples after eucalyptus red staining for 7 and 14 d. After culturing for 7 days, the OD values on the SLA treated Ti and TNZS were higher than those on the flat Ti and TNZS sample surfaces. When the culture time was increased to 14 d, the OD value on the TNZS sample was obviously greater than that on Ti, and the OD value on the SLATNZS sample surface was the highest among all the samples.

3.3 Results of *in vivo* studies

3.3.1 X-ray images. Fig. 4A shows the typical sagittal and axial images of the Ti, TNZS, SLATi and SLATNZS samples after healing in the tibias for 16 weeks. The Ti, TNZS, SLATi and SLATNZS implants were kept at the implanted sites in the tibias. At the implant–bone interface, there was no obvious loosening or dislocation, and no fractures of the tibias surrounding the Ti, TNZS, SLATi and SLATNZS implants occurred, although the implants were in a load-bearing situation. Therefore, the implants had a good mechanical match with the bone.

3.3.2 Micro-CT images. The X-ray technology could not distinguish the fibrous tissue and bone tissue surrounding the implants. Therefore, the micro-CT technique was used to distinguish the bone tissue, soft tissue and the implant. In this work, the bone tissue displayed green, the soft tissue displayed red, and the implant displayed white. Fig. 4B shows the micro-CT colorized pictures for the Ti, TNZS, SLATi and SLATNZS implants from the three viewing directions after implantation for 16 weeks.

It was notable that the biological tissue had coverage shapes that fit well with the implant surface. Some soft tissue marked by white arrows was formed at the Ti implant–bone interface (Fig. 4B(e) and (i)). However, after sand blasting and acid etching, the amount of soft tissue on the SLATi implant surface

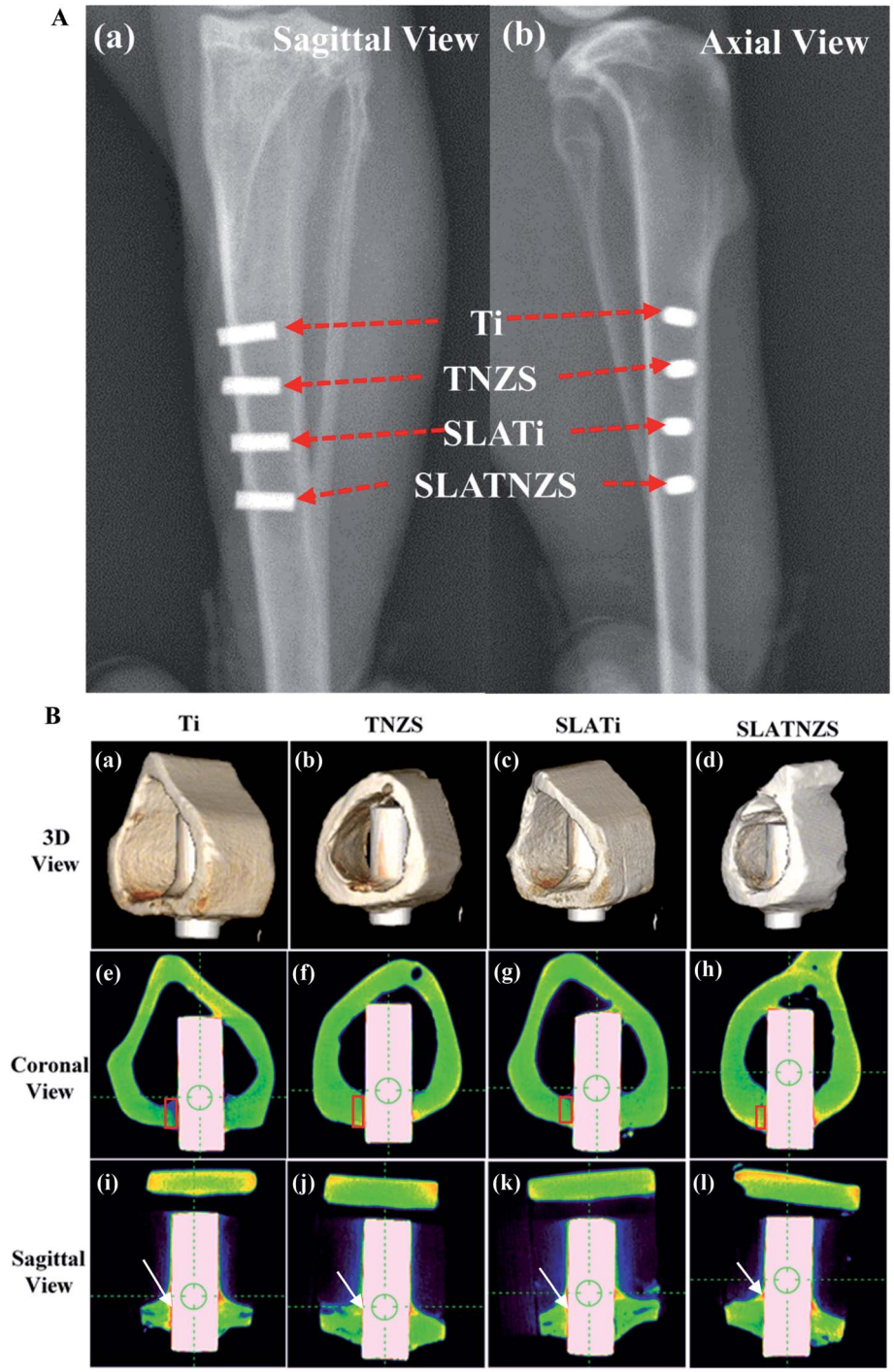

Fig. 4 Data from *in vivo* animal experiments. (A) X-ray images: (a) the sagittal images and (b) the axial image. (B) Micro-CT images: (a)–(d) the 3D reconstruction images for Ti, TNZS, SLATi and SLATNZS implants, respectively, (e)–(h) the coronal images of Ti, TNZS, SLATi and SLATNZS implants, respectively, (i)–(l) the sagittal images of Ti, TNZS, SLATi and SLATNZS implants, respectively. Note: the soft tissue is marked by white arrows, the new bone tissue is marked by a red frame.

was decreased (Fig. 4B(g) and (k)). From the coronal view direction, the bone tissue around the Ti and SLATi implant surfaces was relatively loose. Compared with the Ti implant, a small amount of soft tissue (marked by white arrows) was found at the TNZS and SLATNZS implants and bone interface (Fig. 4B(f), (j) and (h) and (l)). Moreover, as for the TNZS and SLATNZS implant, at the bone–implant interface, the new bone tissue (marked by the red regions in Fig. 4B(e)–(h)) exhibited as relatively dense. The reason for this was attributed to the low modulus and hardness, thus avoiding the absorption of new bone tissue. Meanwhile, there were no cracks observed at the

implant–bone interface for the Ti and TNZS implants before and after sandblasting and acid etching.

The 3D reconstruction results of the bone and soft tissue surrounding the implants after implantation in the tibias for 16 weeks are illustrated in Fig. 5. All the biological tissues had good connection with the implants and completely covered the implants. After healing for 16 weeks, the results of BV/TV and BS/TV revealed that the bone tissue surrounding the SLATNZS implant was the densest, showing excellent osseointegration ability compared to the other implants. Meanwhile, the results also indicated that the low Young's modulus TNZS implant with a porous surface showed excellent osseointegration ability.

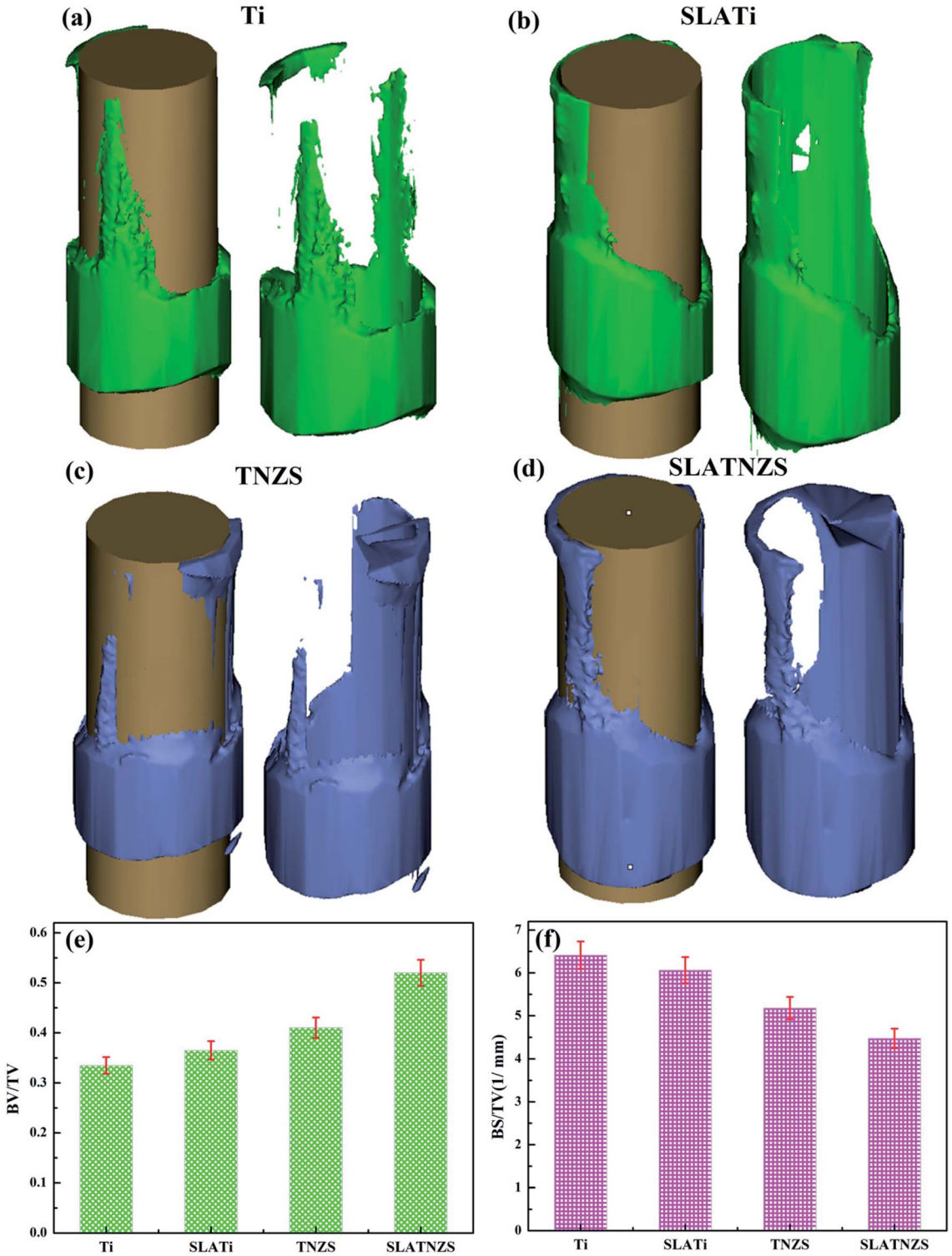

Fig. 5 Micro-CT images: (a), (b), (c) and (d) the 3D reconstruction images for Ti, SLATi, TNZS and SLATNZS implants, (e) BV/TV and (f) BS/TV.

3.3.3 Histological analysis. Fig. 6 shows the histological images of the Ti, TNZS, SLATi and SLATNZS samples after healing in the tibias for 16 weeks. After healing in the tibias for 16 weeks, new bone tissue was formed at the interface between all implants and tissue at the cortical regions (Fig. 4B(a)–(d)). For Ti and SLATi implants (Fig. 6(a) and (b)), it was clear that soft tissue was found around the implant surfaces. But the amounts of soft tissue at the TNZS and SLATNZS implant interfaces were obviously decreased (Fig. 6(c) and (d)).

Moreover, the magnified images exhibited that the Ti implant showed poor connection with the surrounding bone tissue because soft tissue was formed at the interface. Almost no soft tissue was found at the TNZS implant–bone interface, showing a direct contact connection with the bone tissue. After sandblasting and acid etching, it was found that some bone tissue was formed at the cavity on the SLATi and SLATNZS implants, suggesting that the rough surface was beneficial to the growth of bone tissue. Meanwhile, the amount of new bone around the SLATNZS implant was more than that around the SLATi implants.

4. Discussion

As is well known, osseointegration is an important evaluation standard for new bone formation around an implant. During healing, there is some biological interaction between the implant and biological tissue, which involve host bone–implant interaction, and cell–implant interaction. The excellent biological interaction between the implant and biological tissue plays an important role in improving the osseointegration ability of orthopedic implants.[24–26] Recently, some clinical surgeries have revealed that poor osseointegration easily results in a loosening of the implant and subsequent surgical failure.[27,28] To achieve excellent osseointegration ability, many surface modified technologies such as sandblasting and acid etching have been developed. It has been proved that sandblasting is an effective approach to enhancing osseointegration through constructing a rough surface topography. However, after sandblasting, the residual Al_2O_3 can easily affect normal bone mineralization.[29] To avoid this phenomenon, acid etching is effectively applied to remove the residual Al_2O_3 from sandblasting.[30,31] This indicates that the surface modifications could enhance osteoblast response behavior and the formation of new bone tissue.[32,33] In this work, the cell response behavior and *in vivo*

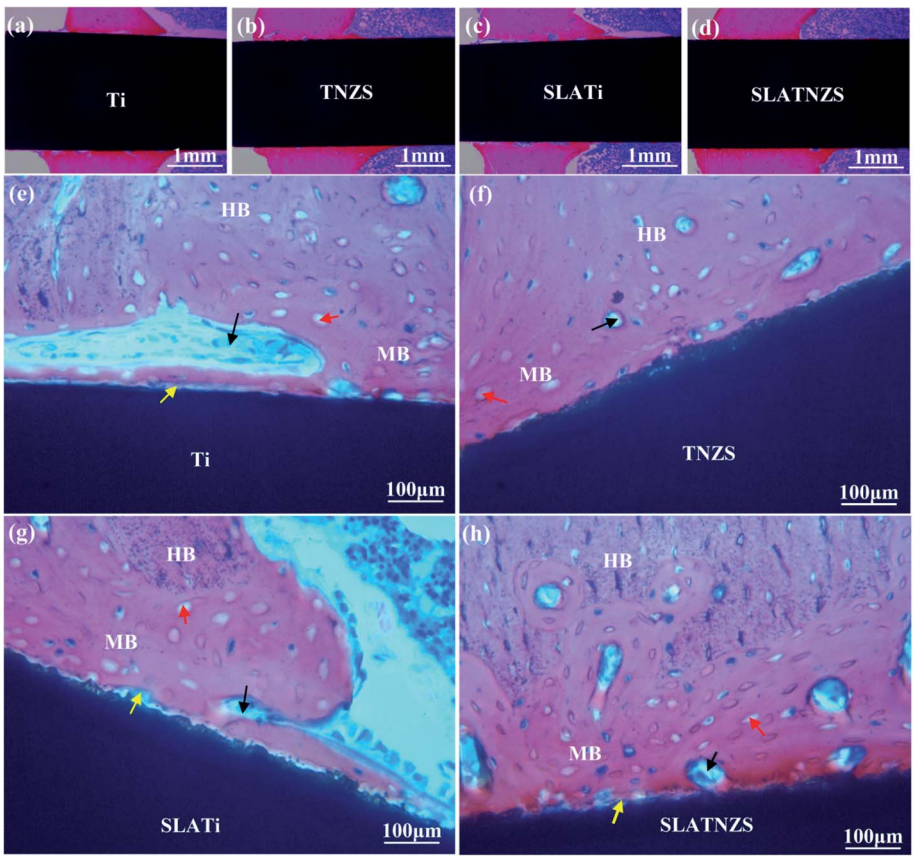

Fig. 6 Histological analysis: (a) the Ti implant, (b) the TNZS implant, (c) the SLATi implant, (d) the SLATNZS implant, (e) the magnified image of the Ti implant, (f) the magnified image of the TNZS implant, (g) the magnified image of the SLATi implant, (h) the magnified image of the SLATNZS implant. Note: MB refers to the mineralized bone, HB refers to the host bone, red arrows refer to the osteocyte, yellow arrows refer to the osteoid, and black arrows refer to the osteoblasts.

osseointegration of the titanium and TNZS before and after sandblasting and acid etching were studied comparatively. The current results suggested that the low Young's modulus porous SLATNZS sample with the micro/nano double scale could synergistically enhance cell proliferation, adhesion and ALP activity *in vitro* and improve osseointegration *in vivo*.

After implantation, the cell–implant interaction took place first in the biological fluid. The interaction ability depended on the surface characters of the implant. The previous study had demonstrated that the cell adhesion mechanism was that the positively charged protein as the intermediate medium enhanced the cell adhesion *via* electrostatic attraction. Generally, cell adhesion behavior often relies on the adhesion and exchange of water molecules and protein. On the hydrophobic and negatively charged surface, in the early stage, the water molecules were firstly absorbed on the implant surface, and were randomly distributed, and then the protein with positive charges was absorbed on the modified titanium surface by releasing the water molecules. Finally, the osteoblast was adhered to the coating surface *via* integration with the membrane protein. However, the superhydrophilic surface could induce the formation of a hydration cation layer *via* hydrogen bonds on the coating surface, which inhibited the absorption of protein, further suppressing the cell response behavior. Thus, the superhydrophilic and superhydrophobic surfaces were both not beneficial to the protein absorption, and then affected the cell behavior response. Although the superhydrophobic surface could greatly affect the absorbed the protein, it could damage the natural conformation of the protein, and further affect cell adhesion. According to the above-mentioned discussion, it was concluded that a biomaterial with a suitable hydrophilic/hydrophobic feature and surface roughness had excellent cell-material interaction with the surrounding biological fluid.

However, in this work, the contact angles on the Ti, SLATi, TNZS and SLATNZS surfaces were similar. The roughness on the SLATi and SLATNZS samples increased compared with the Ti and TNZS samples. Thus, the value of the roughness ranged from 1.7 to 2.2 μm, which was beneficial to cell proliferation, ALP activity and differentiation. Moreover, the previous studies had reported that the matrix stiffness could modify the morphology and focal adhesion characteristics of the cells.[34–36] The surface hardness on TNZS was decreased compared with Ti, and the cell behavior for the TNZS sample was better than that for the Ti sample. The current results were in agreement with the previous studies.

As reported in the previous research, the bone reconstruction and bone resorption around the implant took place simultaneously during healing. Many investigations have indicated that host bone resorption often occurs at the implant–bone interface, which could decrease the stability at the interface and result in surgical failure.[37,38] Besides, the previous studies indicated that a mismatch in the Young's modulus between the implants and host bone tissue could be generated, leading to bone resorption and implant loosening due to stress shielding.[39] Therefore, in this work, to avoid bone resorption and implant loosening at the implant–bone interface, the Ti–24Nb–4Zr–8Sn (TNZS) alloy with a low elastic modulus which was capable of providing a better balance in the Young's modulus between the implant and the bone was studied.[40] The X-ray images showed that all implants remained at the initial implanted sites in the tibias, suggesting that the Ti and TNZS based implants had no loosening or displacement. Based on the BV/TV and BS/TV analysis, the intensity of the bone around the SLATNZS implant was high compared with that around the SLATi implant. These results revealed that the low Young's modulus SLATNZS implant could reduce the "stress shielding" after implantation. Meanwhile, there was little soft tissue around the SLATNZS implant surface, and new bone tissue was also found in the micro-pore region based on the histological analysis and the results of our previous study. However, the resolution of the optical microscopy was very low, and could not be used to judge the size of the pore structure on the alloy surface in Fig. 6. In a future study, we would adopt an ultrathin slice of hard histological tissue to study the interface status, and further reveal whether new bone tissue could grow into the micro-pores.

Based on the current results, Ti–24Nb–4Zr–8Sn (TNZS) is a promising candidate in the field of replacement and repair of hard tissue.

5. Conclusion

In this work, sandblasting and acid etching were successfully applied to change the surface characteristics of Ti and TNZS samples. After sandblasting and acid etching, the surfaces of the Ti and TNZS samples exhibited rough and porous characteristics. Compared with pure Ti, the TNZS alloy had a lower Young's modulus and surface hardness. *In vitro* tests indicated that the SLATNZS sample had better cell adhesion, proliferation, differentiation and ALP activity as compared with pure Ti. Meanwhile, histological analysis indicated that the newly formed bone grew into the micro-pores and almost no soft tissue was found at the implant–bone interface, showing good osseointegration. Therefore, the TNZS alloy as a new implant material is a promising potential candidate in the biochemical field.

Conflicts of interest

The authors declare that they have no Conflicts of interest in this work.

Acknowledgements

This work was financially supported by Heilongjiang Provincial Health Department Project (ZY18C01), Harbin Science and Technology Bureau, the National Natural Science Foundation of China (Grant No. 81771106), National Natural Science Foundation, Innovation Research Group Natural Fund (Grant No. 51621091), Heilongjiang Provincial Youth Science Foundation (QC2013C043), and National Basic Science Research Program (2012CB933900).

References

1 R. I. Asri, W. S. Harun, M. A. Hassan, S. A. Ghani and Z. Buyong, *J. Mech. Behav. Biomed. Mater.*, 2016, **57**, 95–108.
2 P. Tengvall and I. Lundström, *Clin. Mater.*, 1992, **9**, 115–134.
3 L. J. Xu, Y. Y. Chen, Z. G. Liu and F. T. Kong, *J. Alloys Compd.*, 2008, **453**, 320–324.
4 Y. Song, D. S. Xu, R. Yang, D. Li, W. T. Wu and Z. X. Guo, *Mater. Sci. Eng., A*, 1999, **260**, 269–274.
5 P. Majumdar, S. B. Singh and M. Chakraborty, *Mater. Sci. Eng., A*, 2008, **489**, 419–425.
6 Y. L. Hao, S. J. Li, S. Y. Sun, C. Y. Zheng and R. Yang, *Acta Biomater.*, 2007, **3**, 277–286.
7 S. J. Li, T. C. Cui, Y. L. Hao and R. Yang, *Acta Biomater.*, 2008, **4**, 305–317.
8 S. J. Li, Y. W. Zhang, B. B. Sun, Y. L. Hao and R. Yang, *Mater. Sci. Eng., A*, 2008, **480**, 101–108.
9 D. G. Lee, X. Mi, T. K. Eom and Y. Lee, *J. Biomater. Tissue Eng.*, 2016, **6**, 798–801.
10 F. Liu, F. Wang, T. Shimizu, K. Lgarashi and L. Zhao, *Ceram. Int.*, 2006, **32**, 527–531.
11 D. L. Cochran, R. K. Schenk, A. Lussi, F. L. Higginbottom and D. Buser, *J. Biomed. Mater. Res.*, 2015, **40**, 1–11.
12 A. G. I. Rolando, T. Mclachlan, Y. Cai, S. Berner, R. Tannenbaum, Z. Schwartz, K. H. Sandhage and B. D. Boyan, *Biomaterials*, 2011, **32**, 3395–3403.
13 M. Kulkarni, A. Mazare, E. Gongadze, Š. Perutkova, V. Kralj-Iglič, I. Milošev, P. Schmuki, A. Iglič and M. Mozetič, *Nanotechnology*, 2015, **26**, 062002.
14 M. Kulkarni, A. Flašker, M. Lokar, Š. Perutkova, V. Kralj-Iglič, I. Milošev, P. Schmuki, A. Iglič and M. Mozetič, *Int. J. Nanomed.*, 2015, **10**, 1359–1373.
15 D. Kabaso, E. Gongadze, Å. PerutkovÃ, C. Matschegewski, V. Kralj-Iglič, U. Beck, U. van Rienen and A. Iglič, *Comput. Methods Biomech. Biomed. Eng.*, 2011, **14**, 469–482.
16 M. Rezazadeh Shirdar, I. Sudin and M. Taheri, *Vacuum*, 2015, **122**, 82–89.
17 R. Rasouli, A. Barhoum and H. Uludag, *Biomater. Sci.*, 2018, **6**, 1312–1338.
18 T. Sawase, R. Jimbo, K. Baba, Y. Shibata, T. Ikeda and M. Atsuta, *Clin. Oral Implants Res.*, 2010, **19**, 491–496.
19 M. Hannig, L. Kriener, W. Hothhannig, C. Becker-Willinger and H. Schmidt, *J. Nanosci. Nanotechnol.*, 2007, **7**, 4642–4648.
20 D. Wei, Q. Du, S. Guo, D. Jia, Y. Wang, B. Li and Y. Zhou, *Surf. Coat. Technol.*, 2018, **340**, 93–102.
21 R. Zhou, D. Wei, Y. Cao, W. Feng, Q. Du, B. Li, Y. Wang, D. Jia and Y. Zhou, *Mater. Sci. Eng., C*, 2015, **49**, 669–680.
22 Q. Du, D. Wei and S. Wang, *Appl. Surf. Sci.*, 2019, **487**, 708–718.
23 Q. Du, D. Wei, S. Wang, S. Cheng, Y. Wang, B. Li, D. Jia and Y. Zhou, *Chem. Eng. J.*, 2019, **373**, 1091–1110.
24 L. Le Guéhennec, A. Soueidan, P. Layrolle and Y. Amouriq, *Dent. Mater.*, 2007, **23**, 844–854.
25 R. Agarwal and A. J. García, *Adv. Drug Delivery Rev.*, 2015, **94**, 53–62.
26 S. P. Pilipchuk, A. B. Plonka, A. Monje, A. D. Taut, A. Lanis, B. Kang and W. V. Giannobile, *Dent. Mater.*, 2015, **31**, 317–338.
27 S. Kotsovilis, I. K. Karoussis and I. Fourmousis, *Clin. Oral Implants Res.*, 2006, **17**, 587–599.
28 M. Retzepi, M. P. Lewis and N. Donos, *Clin. Oral Implants Res.*, 2010, **21**, 71–79.
29 H. J. Johnson, S. J. Northup, P. A. Seagraves, M. Atallah, P. J. Garvin, L. Lin and T. D. Darby, *J. Biomed. Mater. Res.*, 1985, **19**, 489–508.
30 H. Schliephake, A. Aref, D. Scharnweber, S. Bierbaum and A. Sewing, *Clin. Oral Implants Res.*, 2010, **20**, 38–44.
31 L. Salou, A. Hoornaert, G. Louarn and P. Layrolle, *Acta Biomater.*, 2015, **11**, 494–502.
32 D. Buser, N. Broggini, M. Wieland, R. K. Schenk, A. J. Denzer, D. L. Cochran, B. Hoffmann, A. Lussi and S. G. Steinemann, *J. Dent. Res.*, 2004, **83**, 529–533.
33 I. Abrahamsson, T. Berglundh, E. Linder, N. P. Lang and J. Lindhe, *Clin. Oral Implants Res.*, 2010, **15**, 381–392.
34 S. Fusco, V. Panzetta, V. Embrione and P. A. Netti, *Acta Biomater.*, 2015, **23**, 63–71.
35 Y. Navaro, N. Bleich-Kimelman, L. Hazanov, I. Mironi-Harpaz, Y. Shachaf, S. Garty, Y. Smith, G. Pelled, D. Gazit, D. Seliktar and Z. Gazit, *Biomaterials*, 2015, **49**, 68–76.
36 B. Trappmann, J. E. Gautrot, J. T. Connelly, D. G. Strange, Y. Li, M. L. Oyen, M. A. Cohen Stuart, H. Boehm, B. Li, V. Vogel, J. P. Spatz, F. M. Watt and W. T. Huck, *Nat. Mater.*, 2012, **11**, 642–649.
37 H. Kröger, P. Venesmaa, J. Jurvelin, H. Miettinen, O. Suomalainen and E. Alhava, *Clin. Orthop. Relat. Res.*, 1998, **352**, 66–74.
38 T. Albrektsson and C. Johansson, *Eur. Spine J.*, 2001, **10**, S96–S101.
39 R. Huiskes, H. Weinans and R. B. Van, *Clin. Orthop. Relat. Res.*, 1992, **274**, 124–134.
40 Y. L. Hao, S. J. Li, S. Y. Sun, C. Y. Zheng and R. Yang, *Acta Biomater.*, 2007, **3**, 277–286.